



# Materials and Interfaces

# Data analytics enables significant improvement of robustness in chemical vapor deposition of carbon nanotubes based on vacuum baking

Jaegeun Lee, Moataz Abdulhafez, and Mostafa Bedewy

Ind. Eng. Chem. Res., Just Accepted Manuscript • DOI: 10.1021/acs.iecr.9b01725 • Publication Date (Web): 03 Jun 2019

Downloaded from http://pubs.acs.org on June 7, 2019

#### **Just Accepted**

"Just Accepted" manuscripts have been peer-reviewed and accepted for publication. They are posted online prior to technical editing, formatting for publication and author proofing. The American Chemical Society provides "Just Accepted" as a service to the research community to expedite the dissemination of scientific material as soon as possible after acceptance. "Just Accepted" manuscripts appear in full in PDF format accompanied by an HTML abstract. "Just Accepted" manuscripts have been fully peer reviewed, but should not be considered the official version of record. They are citable by the Digital Object Identifier (DOI®). "Just Accepted" is an optional service offered to authors. Therefore, the "Just Accepted" Web site may not include all articles that will be published in the journal. After a manuscript is technically edited and formatted, it will be removed from the "Just Accepted" Web site and published as an ASAP article. Note that technical editing may introduce minor changes to the manuscript text and/or graphics which could affect content, and all legal disclaimers and ethical guidelines that apply to the journal pertain. ACS cannot be held responsible for errors or consequences arising from the use of information contained in these "Just Accepted" manuscripts.

# Data analytics enables significant improvement of robustness in chemical vapor deposition of carbon nanotubes based on vacuum baking

Jaegeun Lee<sup>1</sup>, Moataz Abdulhafez<sup>1</sup>, and Mostafa Bedewy<sup>1,2,3</sup>\*

<sup>1</sup>Department of Industrial Engineering, University of Pittsburgh, 3700 O'Hara Street, Pittsburgh, PA 15261, USA

<sup>2</sup>Department of Chemical and Petroleum Engineering, University of Pittsburgh, 3700 O'Hara Street, Pittsburgh, PA 15261, USA

<sup>3</sup>Department of Mechanical Engineering and Materials Science, University of Pittsburgh, 3700 O'Hara Street, Pittsburgh, PA 15261, USA

\*author to whom correspondence should be addressed.

E-mail address: mbedewy@pitt.edu (M. Bedewy)

#### Abstract

The root causes underlying run-to-run variations in the synthesis of vertically aligned carbon nanotubes (VACNTs) by chemical vapor deposition can be attributed to the sensitivity of the process to small uncontrolled/unmeasured quantities of gaseous species in the reactor. Hence, universally applicable processing steps are needed to ensure consistency. Here, we quantitatively test the effectiveness of various processing heuristics in reducing growth variability. Statistical analysis of 95 VACNT samples grown by 11 different recipes demonstrated that pumping with mild baking at 200 °C prior to catalyst formation resulted in significantly reduced coefficient of variation of forest heights (by a factor of 6). In contrast, other processing steps such as vacuum pumping without heating and adjusting He to H<sub>2</sub> ratio during catalyst formation did not significantly affect growth variability; we could not reject the null hypothesis at any reasonable level of significance. Atomic force microscopy analyses suggest that variability in VACNT height is not caused by variations of nanoparticle size distribution, thus we can conjecture that the variability might be caused by variations in the chemical state of catalyst nanoparticles.

#### 1. Introduction

Chemical synthesis of nanoparticles, nanotubes, nanowires and other nanostructures has grown over the past several decades to include not only lab-scale research but also commercial production for various new technologies. Promising applications include medical diagnostics and therapeutics, batteries and other energy devices as well as optical and electrical devices. The global nanotechnology market was reported to be US\$ 731 billion in 2012. However, one recurring key challenge in commercialization of nanotechnology is to ensure reproducibility in the scaled production of functional nanostructures and nanomaterials. One root cause of this problem of inconsistency in chemical synthesis typically arises from the sensitivity of chemical reactions to small uncontrolled, and commonly unmeasured, quantities of chemical species in a reactor, particularly in heterogeneous catalysis.

A specific example is the reproducibility issues in the synthesis of carbon nanotubes (CNTs) by chemical vapor deposition (CVD), which have been reported previously. <sup>10–13</sup> Since their discovery, these allotropes of carbon with a hollow cylindrical nanostructure have attracted significant attention due to their superior mechanical, <sup>14</sup> electrical, <sup>15</sup> and thermal <sup>16</sup> properties. These excellent properties of individual CNTs can be fully transferred from the nanoscale to the macroscopic scale when they are assembled into hierarchical and 3D micronscale and macro-scale structures. A vertically aligned CNT array, often referred to as a CNT forest, combines high density and alignment, enabling many applications that leverage their unique anisotropic energy and mass transport properties, such as thermal interfaces <sup>17</sup>, electrical interconnects, <sup>18</sup> flow membranes, <sup>19</sup> and structural materials. <sup>20</sup> However, one roadblock towards the commercial manufacturing of CNT forests is the significant variability typically

reported in CVD growth.<sup>10–13</sup> Run-to-run variations not only overwhelm any efforts for parametric optimization aimed towards tailoring structure and properties, but also severely limit our ability to do fundamental studies of growth kinetics and deactivation mechanisms aimed at catalyst design or revealing the effects of growth promoters. Hence, establishing robust synthesis processes for CNT forests is essential for reliable basic research into collective CNT growth, as well as for the successful commercialization of applications based on CNT forests.

In a typical catalytic CVD reactor, a CNT forest is synthesized from substrate-bound catalyst nanoparticles in an atmosphere containing hydrocarbon gas precursors.  $^{21-29}$  Previous studies have revealed that the main source of variability is oxygen-containing molecules that have uncontrolled low concentrations inside the growth reactor. Hart *et al.* showed that ambient humidity affects the variability of the growth by statistical analysis of 280 samples. Noy *et al.* reported that trace amount of water vapor ( $\sim 1$  ppm) can significantly affect the growth kinetics.  $^{12,30}$  Plata *et al.* showed that different concentrations of oxygen lead to different growth behaviors. They pointed out that a low concentration of oxygen can accelerate the Ostwald ripening of Fe catalyst nanoparticles and this effect can be mitigated by  $H_2$ .

Hence, in order to minimize the uncontrolled effects of all chemical species such as oxygen-containing molecules, some universally applicable processing steps are needed for ensuring the consistency of CNT forest growth by CVD, i.e. we need processing steps that are agnostic to the actual chemical species whose uncontrolled variation underlies growth inconsistency in a way that would work no matter what those species are. Several research groups have reported different types of processing steps prior to the growth such as pumping, <sup>28,32</sup> cycled pumping, <sup>33</sup> heating of gas line with pumping. <sup>34</sup> However, it is still unclear

how effectively these measures contribute to the reduction of variability in the growth of CNT forests, and whether they can be generalized to any CVD reactor. For example, Hart *et al.* demonstrated that rapid insertion of the substrate to the growth environment improves the growth consistency.<sup>11</sup> However, the method requires a special setup (transfer arm sample loading system), which can pose some limitations on the broad application of this method. Moreover, rigorous statistical data analytics is needed to quantify both the reduction of variability and to co-optimize different process parameters that work in unison towards enhancing process robustness.

Here, we present a detailed approach to significantly improve the consistency of CNT forest growth based on combining statistical data analytics with cycling temperature and pressure in a rapid thermal processor. We grew CNT forests with 11 different growth recipes, all of which are derived from one baseline recipe with slight modification to quantitatively test specific hypotheses on growth consistency. Statistical analysis of 95 CNT forests grown using these 11 recipes demonstrated that some small recipe changes such as mild substrate baking at 200 °C with pumping to below 30 mTorr prior to formation of catalyst particles resulted in a statistically significant reduction of growth variability.

#### 2. Experimental

#### 2.1. Custom-designed reactor

For the growth of CNT forests, we used a custom-designed rapid thermal processing (RTP) CVD reactor (CVD Equipment), schematically shown in Fig. 1a. The reactor consists of two adjacent furnaces: a resistive preheater for thermal decomposition of hydrocarbon precursors

(supplied through a coiled injector), and an infrared (IR) heater for catalyst treatment and CNT growth. The IR heater has 3-zone control along the reactor horizontal axis as well as independent control of top and bottom lamps, to create thermal gradients and achieve fast heating (> 50 °C/s). A viewing port enables in situ videography (Fig. 1b). Programmed dynamic recipes are automated, in order to eliminate human errors that could arise during transitioning between successive stages of the process, such as in the case of reactors that include a manual transfer arm. The growth data (e.g. time evolution of temperature, pressure, gas flow rates, etc.) are recorded for analytics, as shown in Fig. 2. A variety of gases (in this work: He, H<sub>2</sub>, and C<sub>2</sub>H<sub>4</sub>) can be used. A diaphragm air pump (Apollo 3000) is used for bakecleaning to remove carbon deposits from the previous growth experiments by heating in air. Special effort was taken to minimize the effect of ambient moisture. A vacuum pump enables pumping down to below 30 mTorr to remove oxygen-containing molecules in the reactor during the purging step. The addition of H<sub>2</sub>O is well controlled via a bubbler with accurate temperature and pressure control. All gas lines are stainless steel, which minimizes the release of oxygen-containing molecules from highly permeable polymer tubing. <sup>10</sup> Further information about the reactor is provided in our previous work.<sup>35</sup>

#### 2.2. Growth of CNT forests

As a substrate for the growth of CNT forests, a silicon wafer with a 300-nm-thick oxide layer was used. A 10-nm-thick  $AlO_x$  film is then deposited by atomic layer deposition, followed by the deposition of 1-nm-thick Fe film by e-beam evaporation. The substrate was cut into small pieces with dimensions of approximately 5 mm  $\times$  5 mm.

Before every growth, we baked the reactor by supplying air into the reactor (using a diaphragm air pump), while heating up to 1000 °C, in order to burn off carbon deposits and remove all

contaminants adsorbed on the reactor wall. After the air baking, a piece of catalyst-coated substrate was loaded into the reactor and a growth was run automatically according to a programmed recipe. A typical recipe used for the growth of CNT forests in this work is described in Fig. 2. All the growth experiments were run at the preheater temperature of 825 °C. In all the recipes, the temperature and pressure of water bubbler were kept at 45 °C and 800 Torr, respectively. The water vapor pressure at this condition is 71.9294 Torr, <sup>36</sup> The He gas flow rate passing through the water bubbler was 200 sccm and the total flow rate was 1700 sccm, so the water vapor concentration at this condition is calculated to be approximately 116 ppm. Most of the recipes had a catalyst formation step that is completely decoupled from the CNT growth step (hereafter referred to as decoupled recipe, Fig. 2), while the other recipes had catalyst formation that is coupled to CNT growth step as in conventional recipes (hereafter referred to as coupled recipe, Fig. S1). Before the catalyst formation step, there were two pumping steps. The first pumping was at the beginning of the recipe and performed without heating. The second pumping was performed when the substrate temperature reached 200 °C due to the heating of the preheater to 825 °C (see Fig. 2). Each recipe had different pumping sequences. Some recipes included only the first pumping step. In general, the first pumping time was either 0.3 or 12 minutes, and the second pumping time was either 10 or 20 minutes.

#### 2.3. Characterization

The height of CNT forests was measured by optical microscopy, as shown in Fig. 3. We collected three height measurements from two sides ("front" and "side"), as shown schematically in Fig. 3a. Commonly, it is assumed that the geometry of a CNT forest is a uniform cuboid and the height of a CNT forest is reported by a single measurement. However, the millimeter-scale forest geometry in many cases exhibits significant non-uniformities, as

shown in Fig. 3b-c. To acquire a more representative measurement for the height of a CNT forest, the geometric non-uniformity needs to be taken into consideration. To achieve this, the overall mean height is calculated by averaging those six values (three from front and three from side view) according to the following definition:

$$\mu_{FH} = \sum_{i=1}^{3} FH_i/3$$

$$\mu_{SH} = \sum_{i=1}^{3} SH_i/3$$

$$\mu_H = \frac{\mu_{FH} + \, \mu_{SH}}{2}$$

, where FH is the height measured from the front, SH is the height measured from the side,  $\mu_{FH}$  is the mean height measured from the front,  $\mu_{SH}$  is the mean height measured from the side, and  $\mu_{H}$  is the overall mean height.

The catalyst nanoparticles after various treatment conditions (without CNT growth) were analyzed by tapping-mode atomic force microscopy (AFM) using Veeco Dimension 3100V. Post processing of the AFM images for obtaining particle size distribution was performed using Gwyddion software (http://www.gwyddion.net). The morphology and structural quality of the as-grown CNT forests were analyzed by scanning electron microscopy (SEM) using JEOL JSM-6510 and Raman spectroscopy (Xplora, Horiba Scientific), respectively.

#### 3. Results and Discussion

# 3.1. Quantifying geometric nonuniformity in forest growth

CVD-grown CNT forests were first characterized by SEM (Fig. 3d-e) and Raman

spectroscopy (Fig. S2). Before analyzing run-to-run variations, we found that it is important to quantify the geometric uniformity within each CNT forest, which is also a metric of the overall robustness of the growth process when these geometric features are not repeatable. As a measure of geometric uniformity of a CNT forest, we use a calculated variable called front-to-side difference ratio (FSDR),

$$FSDR\% = \frac{\mu_{FH} - \mu_{SH}}{\mu_{FH}} \times 100.$$

For perfectly uniform CNT forests, FSDR should always be 0. If the average of FSDR is biased toward positive or negative value, that would indicate a preferential spatial distribution of CNT growth on the same substrate. Such spatial map may arise from undesirable anisotropic temperature profiles or variations in local concentration of precursors, which depend on the reactor design and fluid dynamics. When we measured FSDR of all the CNT forests, FSDR showed a symmetric distribution centered around 0 (Fig. 3f). The narrow distribution of FSDR indicates that there is no significant geometric non-uniformity within a CNT forest. In addition, the symmetry around 0 suggests that there is no significant anisotropic tendency in our CVD reactor that could be attributed to the reactor design, temperature profiles, or flow patterns.

It is also worth noting that the absolute value of FSDR (AFSDR) has a negative correlation with height of a CNT forest (Fig. 3g and Fig. S3). This indicates that, given the same growth condition, uniform growth within a wafer leads to growth of taller CNT forests. This can be attributed to the higher internal mechanical stresses within non-uniform forest growth, which might cause early growth termination, <sup>37,38</sup> even locally.

In addition, Fig. S3 includes histograms of CNT forest heights for samples grown after different pumping times. Although, we can observe that shorter pumping generally leads to shorter

forests, we are more focused in this present work on the effects of processing steps (such a pumping time) on the run-to-run variations in forests height, as opposed to the values of forest height.

# 3.2. Factors affecting run-to-run variations in forest growth

Various factors can potentially influence run-to-run variations in CNT growth by CVD including variability in concentration and transience of specific chemical species, non-repeatability of temperature and flow rates, as well as human error in experimental procedure and sample placement. However, thorough statistical data analytics has not been always employed to test these hypotheses and to quantify the significance of the effects of each independent variable. In this paper, we test several hypotheses based on the assumption that the main source of variability is small uncontrolled concentrations of oxygen-containing molecules in the reactor. We focused on factors that may influence the adsorption of small molecules on, and their diffusion in, the reactor wall. These minute changes to the atmosphere inside the reactor resulting from adsorption/diffusion and outgassing of molecules from the reactor wall can affect the formation of Fe catalyst nanoparticles by thin film dewetting, as well as the catalytic growth of CNT forests. In addition, in an effort to demonstrate the universality of our approach, we also investigate how these factors influence the growth by different types of recipes (coupled and decoupled).

Specifically, we hypothesized that the following four factors may influence the consistency of CNT forest growth by CVD. The first factor was pumping down the reactor to low pressure (below 30 mTorr) before catalyst formation to see if pumping down at room temperature is enough to remove oxygen-containing molecules in the reactor. The second factor is additional pumping to low pressure (below 30 mTorr) with mild baking at 200 °C

before catalyst formation (hereafter referred to as vacuum baking at 200 °C). Since the efficiency of vacuum baking is well known,<sup>39</sup> we hypothesized that heating might be necessary if the vacuum pumping at room temperature is not enough. We chose the temperature during pumping to be 200 °C, which is high enough for effective outgassing from reactor walls, but not too high to affect the catalyst film restructuring or dewetting. The third factor is the temperature of the reactor when it is opened after the air baking recipe (hot open vs. cold open) because temperature-dependent adsorption of small molecules might affect the subsequent growth experiment. Finally, the fourth factor was the ratio of He to H<sub>2</sub> during the catalyst formation step (i.e., He rich vs. H<sub>2</sub> rich). This factor was considered because of previous work showing that the effects of small concentrations of oxygen during catalyst formation can be mitigated by increasing H<sub>2</sub> concentration.<sup>31</sup>

To test the effect of these factors on the consistency of growth, we designed 11 recipes to grow CNT forests as described in Table 1. All recipes share an identical condition for the CNT growth step, but vary in one or more of the four processing factors mentioned above. There are four levels of pumping time: 0.3, 12, 22, and 32 minutes. In the cases of 0.3 and 12 minute pumping, the reactor was pumped down without heating. In the cases of 22 and 32 minute pumping, there was additional pumping at 200 °C for 10 and 20 minutes, respectively (following the first step of pumping without heating). In the He-rich catalyst formation conditions, the flow rate for He and H<sub>2</sub> were 1210 and 490 sccm, respectively, and in the H<sub>2</sub>-rich catalyst formation conditions, the flow rate for He and H<sub>2</sub> were 700 and 1000 sccm, respectively. The temperature for "hot opening" was between 180 and 200 °C, and for "cold opening", below 80 °C. Each recipe was repeated at least 6 times and the number of repeats is indicated in Table 1.

#### 3.3. Quantifying coefficient of variation as a function of pumping time

As a measure of variability of the height between CNT forests grown by each recipe, we relied on the coefficient of variation (CV), defined as the ratio of the standard deviation to the mean. 40 CV is a dimensionless number and a widely used measure of variability because it is not affected by different means of populations or units of measurement, in contrast to standard deviation or variance. The CV values for height of CNT forests obtained from 11 recipes are plotted in Fig. 4. A low CV indicates that the recipe leads to consistent growth results, so the robustness of each recipe can be plotted as a function of pumping time prior to starting the growth recipe. It is noteworthy that with only 0.3 minute pumping, CV was very large (about 0.6). Importantly, our results show that CV decreased by 6-folds (down to about 0.1) in recipes that incorporated vacuum baking at 200 °C.

The dimensionless value of CV is a good metric for quantitatively comparing the robustness of various recipes, and as seen from the six-fold improvement of CV shown in Fig. 4, the improvement is practically significant. However, in order to confirm that these differences between recipes are statistically significant and to identify the significance level, we utilize statistical hypothesis testing. In fact, hypothesis testing is also a useful tool to describe the effects of other non-quantitative processing variable on CV, such as reactor opening temperature and the gas composition during the catalyst formation step.

# 3.4. Statistical hypothesis testing of CV equality

There are several statistical tests for the equality of CV.<sup>41–43</sup> In this work, we used the R package evequality (Version 0.1.3; Marwick and Krishnamoorthy 2019) to test for significant differences in CV.<sup>44</sup> We used two types of tests: asymptotic test developed by Feltz and Miller<sup>41</sup> and modified signed-likelihood ratio test (M-SLRT) developed by

Krishnamoorthy and Lee.<sup>42</sup> The asymptotic test by Feltz and Miller is widely cited as an authoritative test for the equality of CV, and the M-SLRT test was recently developed and has the advantage of having low type I error rates even for sample sizes that are as small as three.<sup>42</sup>

To investigate the effect of pumping time, gas composition during catalyst formation, and reactor opening temperature on CV, we tested the equality of CV for various pairs of recipes as shown in Table 2. The null hypothesis  $(H_0)$  in each case was that the CV for forest heights in the first set of experiments carried out according to recipe i  $(CV_i)$  is equal to the coefficient of variation for forest heights in the other set of experiments carried out according to recipe j  $(CV_j)$ , i.e.  $H_0$ :  $CV_i = CV_j$ . In this case, the alternative hypothesis  $(H_a)$  was that the CV for forest heights in the first set of experiments carried out according to recipe i  $(CV_i)$  is not equal to the CV for forest heights in the other set of experiments carried out according to recipe j  $(CV_j)$ , i.e.  $H_a$ :  $CV_i \neq CV_j$ . The statistic and p-value for each hypothesis test comparing every pair of recipes, from two types of tests, are shown in Table 2.

#### 3.5. Statistically significant improvement in CV for vacuum baking at 200 °C

Results show that a statistically significant difference in CV was observed only when we compared two recipes with different pumping times, according to a significance level of 0.025, which indicates a strong evidence against the null hypothesis. Whenever a recipe with the vacuum baking at 200 °C was compared with one without the vacuum baking at 200 °C, a statistically significant difference in CV at a significance level of 0.02, i.e. the null hypothesis was always rejected regardless of other conditions. However, when 0.3 minute pumping and 12 minute pumping recipes were compared (cold open, decoupled, He-rich), we failed to conclude that there is significant difference in CV (p-value = 0.662 from asymptotic test and 0.632 from M-SLRT), although the CV values seem practically different (CV = 0.688 for 0.3

minute pumping and 0.311 for 12 minute pumping). These results indicate that heating during the pump down at 200 °C plays a crucial role in reducing the variability in CNT forest growth by CVD. On the other hand, pumping down to low pressure (30 mTorr) without heating was not effective enough to reduce growth variability.

#### 3.6. No significant CV improvement for other factors

The other factors including different gas compositions (He/H<sub>2</sub> ratios), and reactor opening temperature after baking did not result in significantly different CV, i.e. the null hypothesis could not be rejected because of high p-values (see Table 2). Three pairs of recipes that had different He/H<sub>2</sub> ratios were compared, but none of them had significantly different CV. One explanation is that the high H<sub>2</sub> concentration during the catalyst formation step is not enough to prevent the run-to-run variation of catalyst formation in the presence of oxygen-containing molecules. Another possibility is that even if the effect of oxygen-containing molecules was effectively mitigated by high H<sub>2</sub> concentration during catalyst formation step, the oxygen-containing molecules could still lead to variability during the CNT growth step. In addition, when four pairs of recipes that differed according to the temperature of the reactor when it is opened after the air baking recipe (cold open vs. hot open) were tested, no statistically significant difference in CV was observed. This implies that the temperature-dependence of adsorption of small molecules is not too significant to affect the growth consistency and that the pumping steps before each recipe are enough to significantly reduce CV, regardless of whether a "cold open" or "hot open" procedure is adopted after baking.

We also studied the difference between coupled recipes and decoupled recipes to test how other factors influence the growth consistency in different types of recipes. The influence of decoupling on CV was dependent on other conditions. For example, in the case of "hot open, 12 min-pumping, and He-rich catalyst formation", the CV of decoupled recipe was significantly higher than that of coupled recipe (p-values underlined in Table 2: 0.0038 from asymptotic test and 0.0075 from M-SLRT) at a level of significance of 0.02. On the contrary, in the case of "cold open, 32-minute pumping, and He-rich catalyst formation", decoupling did not lead to different CV (p-value = 0.652 from asymptotic test and 0.689 from M-SLRT), and we could not reject the null hypothesis at any reasonable level of significance. A possible explanation is that decoupling potentially makes the process more sensitive to variation, which may be due to the extended exposure of the catalyst nanoparticles to the transient conditions during the cooling and heating between the catalyst formation step and the CNT growth step. Importantly, the vacuum baking can make the decoupling recipes more reproducible.

# 3.7. Decoupling the effect of vacuum-baking on nanoparticle size distribution

The vacuum-baking step, which was shown to significantly improve CV, is performed before both the catalyst preparation and the CNT growth steps. Thus, it is necessary to investigate the effects of this vacuum-bake on the resulting nanoparticle size distribution after the catalyst preparation step and before the CNT growth step. We used AFM to characterize the size distribution of catalyst nanoparticles formed after different pumping conditions. To examine the effect of pumping time, we compared two recipes: 0.3 minute pumping and 32 minute pumping with all other conditions being equal (cold open, decoupled, He-rich). For each pumping time, two sets of samples were prepared: For the first set, the recipe was stopped before the first temperature ramp (i.e. before ramping the temperature up to the catalyst preparation temperature); In the second set, the recipe was stopped before the second temperature ramp (i.e. after the catalyst preparation step is over and before ramping the temperature up to the growth temperature). These two sets of samples enabled us to

characterize the distribution of nanoparticles before or after catalyst formation, respectively.

In both the pumping times, before the catalyst formation step, no dewetting of catalyst film was observed (Fig. 5a and c). The surfaces remained flat without forming notable nanoparticles. Importantly, the vacuum baking step at 200 °C did not influence catalyst dewetting, which confirms that the temperature of 200 °C is too low for significant thin film evolution at low pressure.

After the formation of catalyst nanoparticles, the size distributions look different depending on the pumping time (Fig. 5b and d). For the set of samples that were imaged after catalyst formation, we prepared 3 samples per recipe and took 6 AFM images for each sample at different locations for a thorough statistical examination (Fig. S4 and S5). The histogram (Fig. 5e) and box plot (Fig. S6) of the distribution of nanoparticles heights shows a clear shift in the mean size with longer pumping of 32 minutes resulting in smaller nanoparticles than the shorter pumping of 0.3 minutes.

A summary of our quantitative AFM analysis is shown in Table 3, along with statistical analysis and hypothesis testing results. First, we compared the mean values for height of nanoparticles, root mean square (RMS) roughness and number density of nanoparticles, using two-sample Student's t-test. According to the test, the catalyst nanoparticles from 0.3 and 32 minute pumping had significantly different mean heights (p-value = 0.027) and mean RMS roughness (p-value = 0.009) at a level of significance of 0.05. This finding is consistent with previous work by Plata *et al.*, which showed that oxygen promotes Ostwald ripening. The concentration of oxygen-containing species should be higher after 0.3 minute pumping compared to 32 minute pumping resulting in larger nanoparticles.<sup>31</sup> However, the mean number density of nanoparticles did not show a statistically significant difference (p-value = 0.585).

Although there were statistically significant differences in nanoparticle sizes, no significant differences in CV were observed in terms of mean height of nanoparticles, mean RMS roughness, and mean number density of nanoparticles at a level of significance of 0.05 (Table 3). This suggests that the sample-to-sample variability of a CNT forest growth shown earlier in Table 2 does not originate from sample-to-sample variability in the distribution of nanoparticle sizes. Rather, it is more likely that the run-to-run variations among CNT forest heights arise from variations in catalytic activation, CNT nucleation/growth, and catalyst lifetime.

# 3.8. Mechanism of consistency improvement by vacuum baking

Among the various factors tested, only vacuum baking at 200 °C led to significantly reduced variability (both statistically and practically significant differences in CV). In fact, the vacuum baking is a widely used technique to remove water vapor and other volatile contaminants from reactors and deposition chambers.<sup>39</sup> In a reactor, gas molecules are not only present in the internal volume between the walls, but also sticking on the wall by adsorption (and perhaps also moving in the bulk thickness of the wall by diffusion). Under pumping, the gas molecules in the volume are rapidly removed, but those on and in the wall are more difficult to remove. Thus, the rate of diffusion through the wall and the rate of desorption from the wall surface determine effectiveness of any pumping/baking step. The term "outgassing" includes desorption of gas molecules adsorbed to the reactor wall surface and diffusion of gas molecules inside the bulk of the reactor wall towards the surface (Fig. 6a). Diffusion is usually a much slower process than desorption, so the overall outgassing rate is typically governed by the outdiffusion rate. The diffusion constant, D, is a function of temperature, given by  $D = D_0$   $e^{(-E_D/kT)}$ , where  $D_0$  is the maximal diffusion coefficient,  $E_D$  is the activation energy for

diffusion, k is the Boltzmann constant, and T is the absolute temperature. Due to the exponential dependence on temperature, a modest increase in temperature sharply increases outdiffusion rate as described in Fig. 6b. Here, we quantitatively estimate the difference of outgassing rates at different temperatures, assuming a uniform initial concentration of dissolved gas in a wall. The outgassing rate, q, can be expressed as

$$q = C_0 \left(\frac{D}{\pi t}\right)^{1/2} \left[ 1 + 2 \sum_{1}^{\infty} (-1)^n \exp\left(\frac{-n^2 d^2}{Dt}\right) \right],$$

where 2d is the thickness of the material,  $C_0$  is the internal pressure of the gas dissolved in the solid.<sup>39</sup> The outgassing rate equation is obtained by solving the diffusion equation. In Fig. 6c, we plotted the outgassing rates with two different diffusion coefficients of water through silica glass:  $D = 10^{-18}$  m<sup>2</sup> s<sup>-1</sup> at 25 °C and  $D = 10^{-14.5}$  m<sup>2</sup> s<sup>-1</sup> at 200 °C.<sup>46</sup>

The outgassing rate is reported in unites of Pa.m.s<sup>-1</sup> and can be converted into diffusion flux units.<sup>47</sup> The plot indicates that the initial outgassing rate is faster at 200 °C than at 25 °C more than 100 times, as can be expected from the huge difference in diffusion coefficients. Hence, the vacuum baking at 200 °C effectively removes oxygen-containing molecules before starting the growth recipe, in effect "resetting" the conditions in the reactor before catalyst preparation and CNT growth steps. The results are consistent with the previous reports that the growth of CNT forest by CVD is exceedingly sensitive that even ppm level of oxygen-containing molecules can significantly influence the growth.<sup>10,12,22,30,31</sup>

#### 3.9. Scientific origins of CNT growth consistency improvement

The trace amounts of oxygen-containing molecules may influence the two steps of the growth: the catalyst formation step and the CNT growth step. When we consider the catalyst

formation step first, the AFM results suggest that the sample-to-sample variability of a CNT forest growth does not originate from sample-to-sample variability in the distribution of nanoparticles. Instead, we should consider the chemical effects during catalyst formation. In fact, for a nanoparticle to have catalytic activity for CNT growth, proper chemical state<sup>48–52</sup> as well as appropriate size<sup>53</sup> are required. Especially, it is known that oxidation state of the catalyst plays a key role in the growth of CNT forests. Hofmann *et al.* showed that for Fe, the active state of the catalyst is a crystalline metallic nanoparticle, not the oxide.<sup>50,51</sup> Teblum *et al.* investigated the effect of oxidation state of Fe on the growth of CNT forests by tuning the catalyst pretreatment processes with different gas-phase environment and found that the most reductive environment during catalyst pretreatment processes yields the most efficient growth.<sup>52</sup> Because of the dependence of catalytic activity on the oxidation state of catalyst nanoparticles, thorough control of oxygen-containing molecules inside the reactor is of critical importance for CNT forest growth.

The high sensitivity of CNT growth kinetics to oxygen-containing molecules has also been previously observed by Noy *et al.*<sup>12,30</sup> In those reports, even 1 ppm level of water vapor significantly affected the growth kinetics. In fact, impurities issue has long been an inherent limitation in atmospheric pressure CVD (APCVD) as compared to low pressure CVD.<sup>54</sup> For example, it has been recently shown that in the synthesis of graphene using APCVD, sub-ppm levels of residual oxygen-containing impurities significantly influence the synthesis reaction by oxidatively etching the graphene.<sup>55,56</sup> Since the CNT nucleation step, wherein carbon atoms self-organize on the surface of catalyst nanoparticles before CNT lift-off, shares similar physicochemical pathways with graphene synthesis, similar etching processes induced by oxygen-containing impurities might also influence the CNT nucleation step, leading to

inconsistency of nucleation density, growth rates, and catalytic lifetime growth. Thus, the improved consistency of CNT forest growth achieved by the vacuum-baking that we observe in this work is likely resulting from improved consistency in chemical atmosphere inside the reactor during both catalyst formation and CNT growth steps. In particular, we demonstrate an improved process robustness, resulting from the reduced variability in small uncontrolled concentrations of oxygen containing molecules, such as H<sub>2</sub>O and O<sub>2</sub>.

#### 4. Conclusion

We use statistical data analytics to aid in the decision making regarding processing steps aimed at reducing run-to-run variations in the growth of CNT forests by catalytic CVD. Based on the hypothesis that the growth inconsistency mainly originates from small uncontrolled concentrations of oxygen-containing molecules in the reactor, we tested the effects of four factors on run-to-run variations: (1) pumping before catalyst formation, (2) additional vacuum baking at 200 °C before catalyst formation, (3) the temperature of the reactor when it is opened after the air baking recipe, and (4) the ratio of He to H<sub>2</sub> during the catalyst formation step. Besides, we tested how these factors affect the run-to-run variation in different types of recipes (coupled and decoupled). To test the effect of these factors, we designed 11 recipes and statistically analyzed the results for 95 CNT forests. Among the four factors, only the vacuum baking at 200 °C led to a decrease in variability that is both statistically and practically significant. By AFM analyses, we confirmed that the vacuum baking did not cause dewetting of catalyst film. On the other hand, when we compared the nanoparticle size distribution after catalyst formation no significant difference in variability was observed for nanoparticle height or number density. Based on the AFM analyses, we can conjecture that run-to-run variations

in CNT forest growth arises from sensitivity to chemical state of catalyst nanoparticles to small uncontrolled concentration of oxygen containing species, rather than variability in size distribution or number density of nanoparticles. The vacuum-baking approach is applicable to other CVD synthesis of nanomaterials such as graphene and various nanowires where a careful control of chemical composition of gaseous species inside the reactor is required before the fabrication process.

#### Acknowledgements

This research was supported by the National Science Foundation (NSF) (Award Number:1825772) and the Department of Industrial Engineering at the University of Pittsburgh. M. Bedewy is grateful for the Ralph E. Powe Junior Faculty Enhancement Award from Oak Ridge Associated Universities (ORAU). Characterization was performed, in part, at the Nanoscale Fabrication and Characterization Facility, a laboratory of the Gertrude E. and John M. Petersen Institute of NanoScience and Engineering, housed at the University of Pittsburgh, and in part, at Materials Characterization Laboratory, housed at Department of Chemistry in the University of Pittsburgh.

# **Supporting Information**

Description of coupled growth recipe used in this work. Raman spectrum of CVD-grown CNT forest. Front-side difference ratio with respect to height of CNT forests. AFM images for catalyst nanoparticles with data analysis.

#### References

- (1) Boisselier, E.; Astruc, D. Gold Nanoparticles in Nanomedicine: Preparations, Imaging, Diagnostics, Therapies and Toxicity. *Chem. Soc. Rev.* **2009**, *38* (6), 1759–1782.
- (2) Bruce, P. G.; Scrosati, B.; Tarascon, J.-M. Nanomaterials for Rechargeable Lithium Batteries. *Angew. Chemie Int. Ed.* **2008**, *47* (16), 2930–2946.
- (3) Guo, Y. G.; Hu, J. S.; Wan, L. J. Nanostructured Materials for Electrochemical Energy Conversion and Storage Devices. *Adv. Mater.* **2008**, *20* (15), 2877–2887.
- (4) Yan, R.; Gargas, D.; Yang, P. Nanowire Photonics. *Nat. Photonics* **2009**, *3* (10), 569–576.
- (5) Kind, H.; Yan, H. Q.; Messer, B.; Law, M.; Yang, P. D. Nanowire Ultraviolet Photodetectors and Optical Switches. *Adv. Mater.* **2002**, *14* (2), 158–160.
- (6) Colinge, J. P.; Lee, C. W.; Afzalian, A.; Akhavan, N. D.; Yan, R.; Ferain, I.; Razavi, P.; O'Neill, B.; Blake, A.; White, M.; et al. Nanowire Transistors without Junctions. *Nat. Nanotechnol.* 2010, 5 (3), 225–229.
- (7) No Title https://www.nsf.gov/news/news\_summ.jsp?cntn\_id=130586 (accessed Feb 18, 2019).
- (8) Mazzola, L. Commercializing Nanotechnology. *Nat. Biotechnol.* **2003**, *21* (10), 1137–1143.
- (9) Kaur, I. P.; Kakkar, V.; Deol, P. K.; Yadav, M.; Singh, M.; Sharma, I. Issues and Concerns in Nanotech Product Development and Its Commercialization. *J. Control. Release* 2014, 193 (2014), 51–62.

- (10) Oliver, C. R.; Polsen, E. S.; Meshot, E. R.; Tawfick, S.; Park, S. J.; Bedewy, M.; Hart, A. J. Statistical Analysis of Variation in Laboratory Growth of Carbon Nanotube Forests and Recommendations for Improved Consistency. ACS Nano 2013, 7 (4), 3565–3580.
- (11) Li, J.; Bedewy, M.; White, A. O.; Polsen, E. S.; Tawfick, S.; John Hart, A. Highly Consistent Atmospheric Pressure Synthesis of Carbon Nanotube Forests by Mitigation of Moisture Transients. *J. Phys. Chem. C* 2016, *120* (20), 11277–11287.
- (12) In, J. Bin; Grigoropoulos, C. P.; Chernov, A. A.; Noy, A. Growth Kinetics of Vertically Aligned Carbon Nanotube Arrays in Clean Oxygen-Free Conditions. ACS Nano 2011, 5 (12), 9602–9610.
- (13) Liu, K.; Liu, P.; Jiang, K.; Fan, S. Effect of Carbon Deposits on the Reactor Wall during the Growth of Multi-Walled Carbon Nanotube Arrays. *Carbon N. Y.* 2007, 45 (12), 2379–2387.
- (14) Yu, M.; Yu, M.; Lourie, O.; Dyer, M. J.; Moloni, K.; Kelly, T. F.; Ruoff, R. S. Strength and Breaking Mechanism of Multiwalled Carbon Nanotubes Under Tensile Load. *Science* **2000**, *287* (2000), 637–640.
- (15) Ebbesen, T. W.; Lezec, H. J.; Hiura, H.; Bennett, J. W.; Ghaemi, H. .; Thio, T. Electrical Conductivity of Individual Carbon Nanotubes. *Nature*. 1996, pp 54–56.
- (16) Berber, S.; Kwon, Y.-K.; Tomanek, D. Unusually High Thermal Conductivity of Carbon Nanotubes. *Phys. Rev. Lett.* **2000**, *84* (20), 4613–4616.
- (17) Soga, I.; Kondo, D.; Yamaguchi, Y.; Iwai, T.; Kikkawa, T.; Joshin, K. Thermal Management for Flip-Chip High Power Amplifiers Utilizing Carbon Nanotube Bumps. 2009 IEEE Int. Symp. Radio-Frequency Integr. Technol. RFIT 2009 2009, 221–224.

- (18) Vanpaemel, J.; Sugiura, M.; Barbarin, Y.; De Gendt, S.; Tökei, Z.; Vereecken, P. M.; van der Veen, M. H. Growth and Integration Challenges for Carbon Nanotube Interconnects. *Microelectron. Eng.* 2014, 120, 188–193.
- Holt, J. K.; Park, H. G.; Wang, Y.; Stadermann, M.; Artyukhin, A. B.; Grigoropoulos,
   C. P.; Noy, A.; Bakajin, O. Fast Mass Transport Through Sub-2-Nanometer Carbon
   Nanotubes. *Science* 2006, 312 (5776), 1034–1037.
- (20) Liang, X.; Shin, J.; Magagnosc, D.; Jiang, Y.; Jin Park, S.; John Hart, A.; Turner, K.; Gianola, D. S.; Purohit, P. K. Compression and Recovery of Carbon Nanotube Forests Described as a Phase Transition. *Int. J. Solids Struct.* 2017, 122–123, 196–209.
- (21) W. Z., G. L.; S. S., X.; Qian L.X.; B. H., C.; Zou B. S.; W. Y., Z.; Wang, Z. R. A. Large-Scale Synthesis of Aligned Carbon Nanotubes. *Science* **1996**, *274* (5293), 1701–1703.
- (22) Hata, K.; Futaba, D. N.; Mizuno, K.; Namai, T.; Yumura, M.; Iijima, S. Water-Assisted Highly Efficient Synthesis of Impurity-Free Single-Walled Carbon Nanotubes. *Science* **2004**, *306* (5700), 1362–1364.
- (23) Zhang, X.; Jiang, K.; Feng, C.; Liu, P.; Zhang, L.; Kong, J.; Zhang, T.; Li, Q.; Fan, S. Spinning and Processing Continuous Yarns from 4-Inch Wafer Scale Super-Aligned Carbon Nanotube Arrays. Adv. Mater. 2006, 18 (12), 1505–1510.
- (24) Bedewy, M.; Meshot, E. R.; Reinker, M. J.; Hart, A. J. Population Growth Dynamics of Carbon Nanotubes Population Growth Dynamics of Carbon Nanotubes. ACS Nano 2011, No. 11, 8974–8989.
- (25) Cho, W.; Schulz, M.; Shanov, V. Growth and Characterization of Vertically Aligned Centimeter Long CNT Arrays. *Carbon N. Y.* **2014**, *72*, 264–273.

- (26) Lee, J.; Oh, E.; Kim, T.; Sa, J. H.; Lee, S. H.; Park, J.; Moon, D.; Kang, I. S.; Kim, M. J.; Kim, S. M.; et al. The Influence of Boundary Layer on the Growth Kinetics of Carbon Nanotube Forests. *Carbon N. Y.* **2015**, *93*, 217–225.
- (27) Bedewy, M. Data-Driven Understanding of Collective Carbon Nanotube Growth by in Situ Characterization and Nanoscale Metrology. *J. Mater. Res.* **2017**, *32* (01), 153–165.
- (28) Youn, S. K.; Frouzakis, C. E.; Gopi, B. P.; Robertson, J.; Teo, K. B. K.; Park, H. G. Temperature Gradient Chemical Vapor Deposition of Vertically Aligned Carbon Nanotubes. *Carbon N. Y.* 2013, 54, 343–352.
- (29) Fan, S.; Chapline, M. G.; Franklin, N. R.; Tombler, T. W.; Cassell, A. M.; Dai, H. Self-Oriented Regular Arrays of Carbon Nanotubes and Their Field Emission Properties. *Science* **1999**, *283* (5401), 512–514.
- (30) In, J. Bin; Grigoropoulos, C. P.; Chernov, A. A.; Noy, A. Hidden Role of Trace Gas Impurities in Chemical Vapor Deposition Growth of Vertically-Aligned Carbon Nanotube Arrays. *Appl. Phys. Lett.* 2011, 98 (15), 153102.
- (31) Shi, W.; Li, J.; Polsen, E. S.; Oliver, C. R.; Zhao, Y.; Meshot, E. R.; Barclay, M.; Fairbrother, D. H.; Hart, A. J.; Plata, D. L. Oxygen-Promoted Catalyst Sintering Influences Number Density, Alignment, and Wall Number of Vertically Aligned Carbon Nanotubes. *Nanoscale* 2017, 9, 5222–5233.
- (32) Yang, N.; Youn, S. K.; Frouzakis, C. E.; Park, H. G. An Effect of Gas-Phase Reactions on the Vertically Aligned CNT Growth by Temperature Gradient Chemical Vapor Deposition. *Carbon N. Y.* **2018**, *130*, 607–613.
- (33) Qi, H.; Yuan, D.; Liu, J. Two-Stage Growth of Single-Walled Carbon Nanotubes. J.

- Phys. Chem. C 2007, 111 (17), 6158-6160.
- (34) Amama, P. B.; Pint, C. L.; McJilton, L.; Kim, S. M.; Stach, E. a; Murray, P. T.; Hauge, R. H.; Maruyama, B. Role of Water in Super Growth of Single-Walled Carbon Nanotube Carpets. *Nano Lett.* **2009**, *9* (1), 44–49.
- (35) Lee, J.; Abdulhafez, M.; Bedewy, M. Multizone Rapid Thermal Processing to Overcome Challenges in Carbon Nanotube Manufacturing by Chemical Vapor Deposition. J. Manuf. Sci. Eng. 2019.
- (36) Lide, D. R. CRC Handbook of Chemistry and Physics, 85th ed.; CRC Press, 2004.
- (37) Bedewy, M.; Hart, A. J. Mechanical Coupling Limits the Density and Quality of Self-Organized Carbon Nanotube Growth. *Nanoscale* **2013**, *5* (7), 2928.
- (38) Han, J. H.; Graff, R. A.; Welch, B.; Marsh, C. P.; Franks, R.; Strano, M. S. A Mechanochemical Model of Growth Termination in Vertical Carbon Nanotube Forests. *ACS Nano* **2008**, *2* (1), 53–60.
- (39) O'Hanlon, J. F. *A User's Guide to Vacuum Techolonogy*, 3rd ed.; John Wiley & Sons, Inc.: Hoboken, NJ, USA, 2003.
- (40) Pearson, K. Mathematical Contributions to the Theory of Evolution . III . Regression , Heredity , and Panmixia Author (s): Karl Pearson Source: Philosophical Transactions of the Royal Society of London . Series A , Containing Papers of a Mathematical or Physical C. Philos. Trans. R. Soc. London. Ser. A, Contain. Pap. a Math. or Phys. Character 1896, 187 (1896), 253–318.
- (41) FELTZ, C. J.; MILLER, G. E. AN ASYMPTOTIC TEST FOR THE EQUALITY OF

- COEFFICIENTS OF VARIATION FROMk POPULATIONS. *Stat. Med.* **1996**, *15* (6), 647–658.
- (42) Krishnamoorthy, K.; Lee, M. Improved Tests for the Equality of Normal Coefficients of Variation. *Comput. Stat.* **2014**, *29* (1–2), 215–232.
- (43) T, A. K.; K, A. R. Pairwise Comparison of Coefficients of Variation for Correlated Samples. *Int. J. Stat. Appl.* **2015**, *5* (5), 231–236.
- (44) Marwick, B.; Krishnamoorthy, K. evequality: Tests for the Equality of Coefficients of Variation from Multiple Groups, R software package version 0.1.3.
- (45) Petruccelli, J. D.; Nandram, B.; Chen, M. *Applied Statistics for Engineers and Scientists*; Prentice Hall New Jersey, 1999.
- (46) K.M., Davis; M., T. Water Diffusion into Silica Glass: Structural Changes in Silica Glass and Their Effect on Water Solubility and Diffusivity. *J. Non. Cryst. Solids* **1995**, *185*, 203–220.
- (47) Redhead, P. A. Recommended Practices for Measuring and Reporting Outgassing Data. *J. Vac. Sci. Technol. A Vacuum, Surfaces, Film.* **2002**, *20* (5), 1667–1675.
- (48) Deck, C. P.; Vecchio, K. Prediction of Carbon Nanotube Growth Success by the Analysis of Carbon-Catalyst Binary Phase Diagrams. *Carbon N. Y.* **2006**, *44* (2), 267–275.
- (49) Mazzucco, S.; Wang, Y.; Tanase, M.; Picher, M.; Li, K.; Wu, Z.; Irle, S.; Sharma, R. Direct Evidence of Active and Inactive Phases of Fe Catalyst Nanoparticles for Carbon Nanotube Formation. *J. Catal.* 2014, 319, 54–60.

- (50) Hofmann, S.; Blume, R.; Wirth, C. T. C. T.; Cantoro, M.; Sharma, R.; Ducati, C.; Hävecker, M.; Zafeiratos, S.; Schnoerch, P.; Oestereich, A.; et al. State of Transition Metal Catalysts During Carbon Nanotube Growth. *J. Phys. Chem. C* 2009, *113* (5), 1648–1656.
- (51) Mattevi, C.; Wirth, C. T.; Hofmann, S.; Blume, R.; Cantoro, M.; Ducati, C.; Cepek, C.; Knop-Gericke, A.; Milne, S.; Castellarin-Cudia, C.; et al. In-Situ X-Ray Photoelectron Spectroscopy Study of Catalyst–Support Interactions and Growth of Carbon Nanotube Forests. J. Phys. Chem. C 2008, 112 (32), 12207–12213.
- (52) Teblum, E.; Gofer, Y.; Pint, C. L.; Nessim, G. D. Role of Catalyst Oxidation State in the Growth of Vertically Aligned Carbon Nanotubes. *J. Phys. Chem. C* **2012**, *116* (46), 24522–24528.
- (53) Lu, C.; Liu, J. Controlling the Diameter of Carbon Nanotubes in Chemical Vapor Deposition Method by Carbon Feeding. *J. Phys. Chem. B* **2006**, *110* (41), 20254–20257.
- (54) Seshan, K.; Schepis, D. Handbook of Thin Film Deposition; Elsevier, 2018.
- (55) Choubak, S.; Biron, M.; Levesque, P. L.; Martel, R.; Desjardins, P. No Graphene Etching in Purified Hydrogen. *J. Phys. Chem. Lett.* **2013**, *4* (7), 1100–1103.
- (56) Felten, A.; Santos, C. N.; Reckinger, N.; Colomer, J.-F.; Hackens, B. The Influence of Residual Oxidizing Impurities on the Synthesis of Graphene by Atmospheric Pressure Chemical Vapor Deposition. *Carbon N. Y.* **2013**, *63*, 84–91.

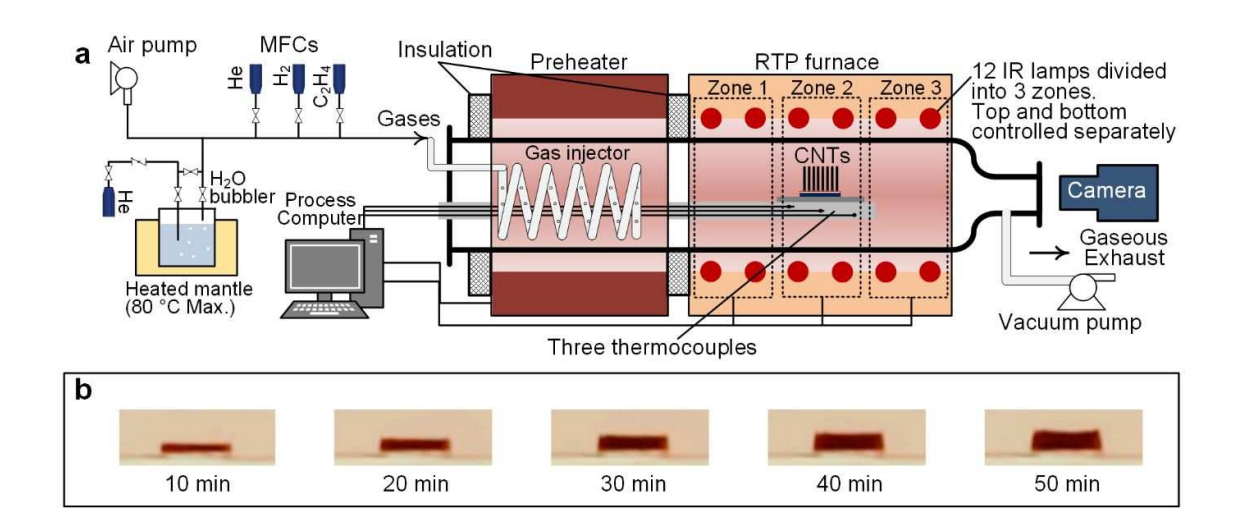


Fig. 1. (a) Schematic representation of the RTP CVD reactor used in this work. (b) Snapshots of a CNT forest growing in the reactor recorded by the video camera (sample size  $\approx 10 \times 10$  mm<sup>2</sup>).

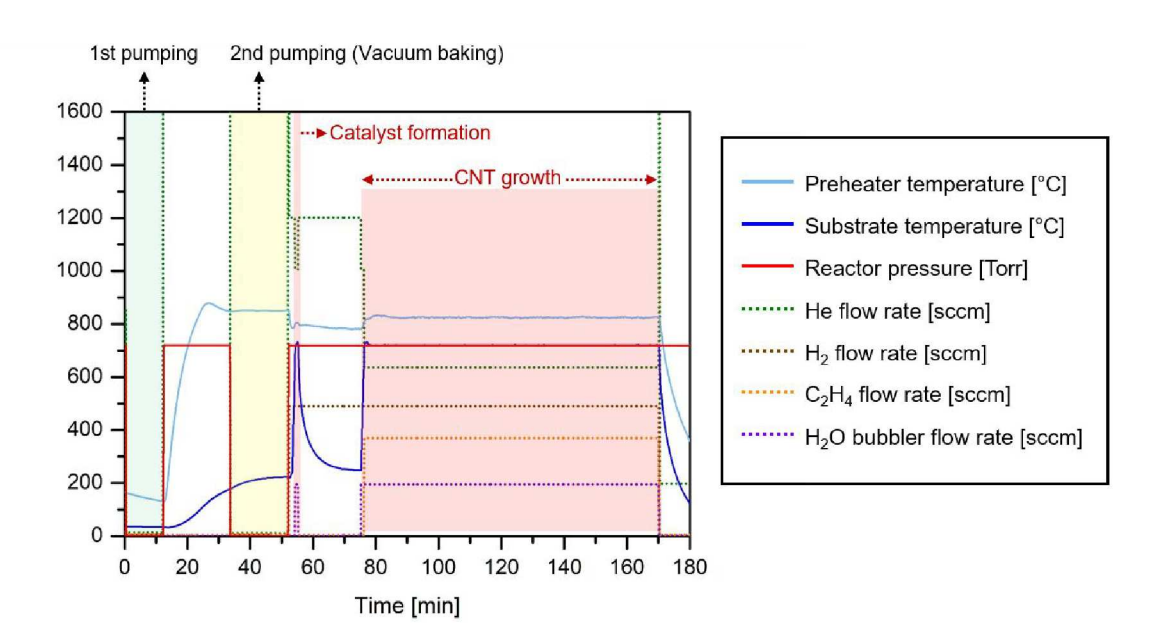


Fig. 2. A typical decoupled dynamic recipe used in this work. The recipe includes first pumping, second pumping at around 200 °C, a decoupled catalyst formation step, and CNT growth step.

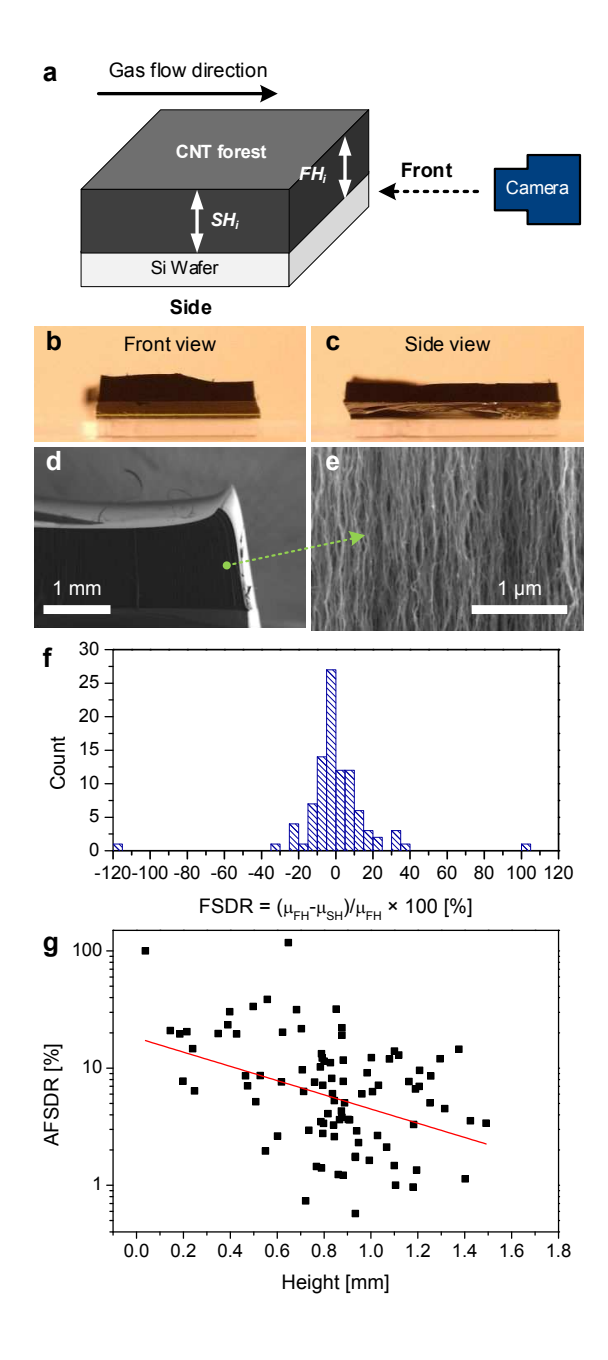


Fig. 3. (a) Schematic showing the forest height measurements from two different sides. (b) Front and (c) side view optical image of a typical CNT forest. (d, e) SEM images of a typical CNT forest. (f) Histogram of FSDR of CNT forests. (g) Plot of absolute values of FSDR as a function of forest height, showing the negative correlation. The red line is the linear regression line ( $R^2 = 0.116$ ).

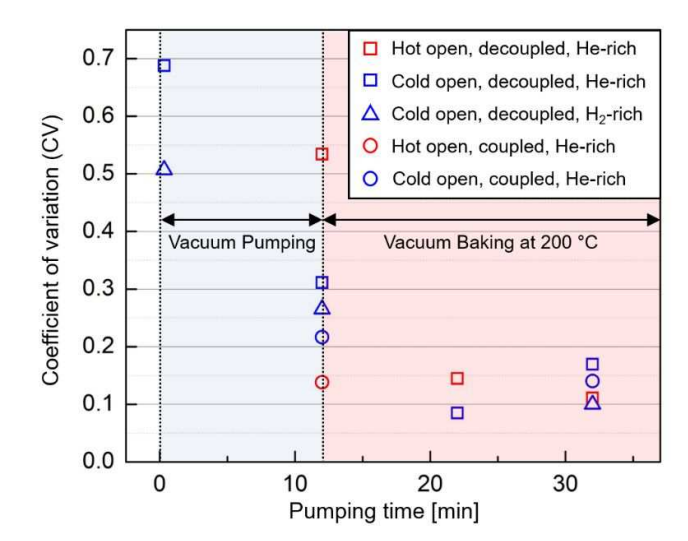


Fig. 4. CV of height of CNT forests synthesized from various growth recipes described in Table 1.

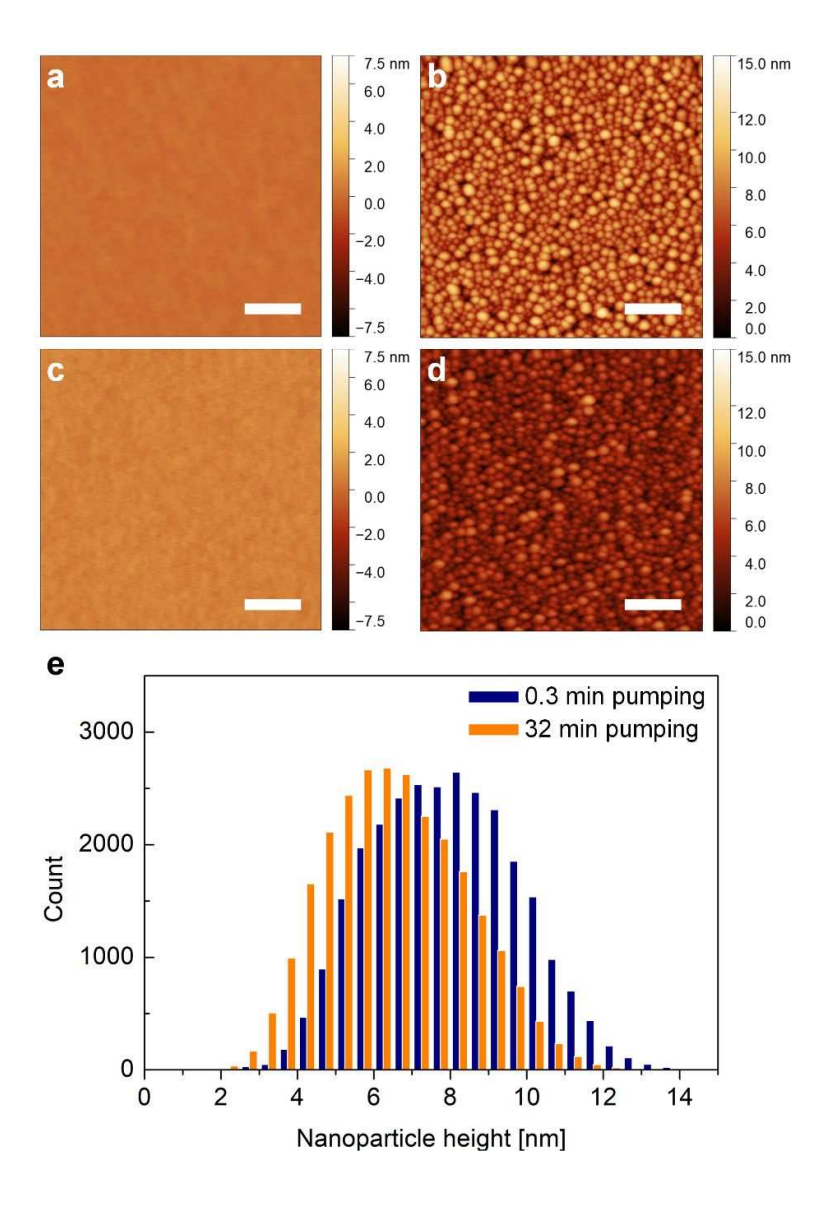


Fig. 5. (a, b) Representative AFM images of substrates after different treatments after pumping down for 0.3 minutes: (a) before catalyst preparation step and (b) after catalyst preparation step. (c, d) Representative AFM images of substrates after different treatments after pumping down for 32 minutes: (c) before catalyst preparation step and (d) after catalyst preparation step. Scale bars are 200 nm. (e) Histogram of nanoparticle heights after the catalyst preparation step for different pumping times (0.3 and 32 minutes).

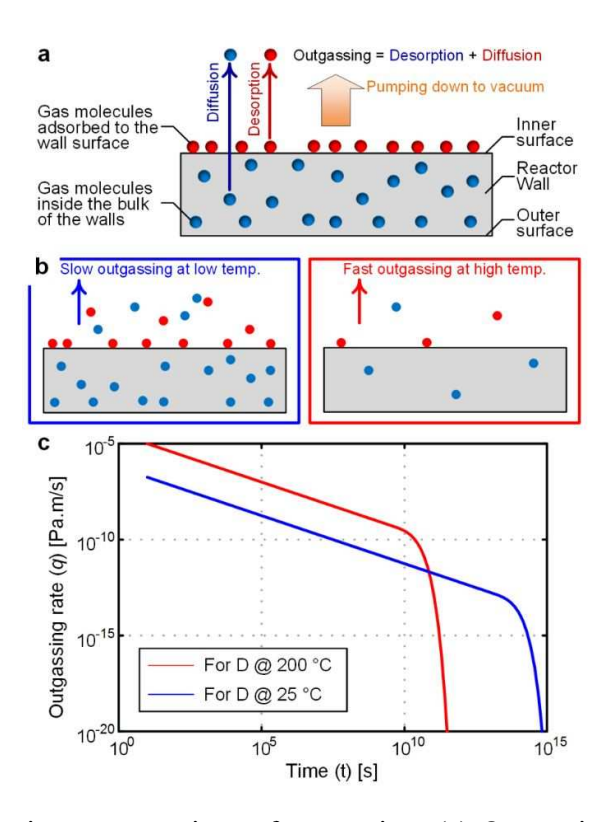


Fig. 6. (a)-(b) Schematic representations of outgassing: (a) Outgassing includes desorption from the wall surface and diffusion from inside the bulk of the wall; (b) Slow outgassing at low temperature and fast outgassing at high temperature. (c) Outgassing rate vs. time with two different diffusion coefficients:  $D = 10^{-18}$  m<sup>2</sup> s<sup>-1</sup> at 25 °C and  $D = 10^{-14.5}$  m<sup>2</sup> s<sup>-1</sup> at 200 °C. The diffusion coefficients are estimates for water diffusion through silica glass. For the calculation, we assumed  $C_0 = 10^5$  Pa and  $d = 10^{-4}$  m.

Table 1. Description of recipes and statistics obtained from the growths by each recipe.

Description of recipe	Average height [mm]	Standard deviation [mm]	Coefficient of variation (CV)	Number of samples
Decoupled, He-rich annealing, 0.3-pumping, Cold-open	0.39	0.27	0.69	7
Decoupled, H <sub>2</sub> -rich annealing, 0.3-pumping, Cold-open	0.31	0.16	0.51	7
Decoupled, He-rich annealing, 12-pumping, Hot-open	0.90	0.48	0.53	6
Decoupled, He-rich annealing, 12-pumping, Cold-open	0.72	0.22	0.31	7
Decoupled, He-rich annealing, 22 min- pumping, Hot-open	1.16	0.17	0.14	7
Decoupled, He-rich annealing, 22 min- pumping, Cold-open	1.25	0.11	0.08	6
Decoupled, He-rich annealing, 32 min- pumping, Hot-open	0.80	0.09	0.11	7
Decoupled, He-rich annealing, 32 min- pumping, Cold-open	0.92	0.16	0.17	7
Decoupled, H <sub>2</sub> -rich annealing, 12-pumping, Cold-open	0.77	0.20	0.27	9
Decoupled, H <sub>2</sub> -rich annealing, 32 min- pumping, Cold-open	0.75	0.08	0.10	7
Coupled, He-rich annealing, 12-pumping, Hot-open	1.03	0.14	0.14	8
Coupled, He-rich annealing, 12-pumping, Cold-open	0.98	0.21	0.22	10
Coupled, He-rich annealing, 32-	0.81	0.11	0.14	7

pumping, Cold-open				
--------------------	--	--	--	--

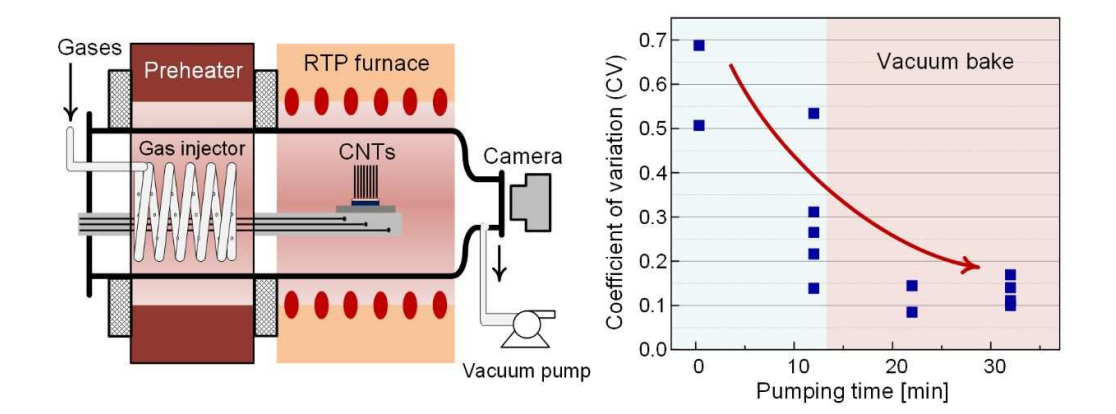
Table 2. Results of statistical tests for equality of CV of height of CNT forest. The recipes with different pumping time, gas composition during catalyst formation, and reactor opening temperature were compared. P-values less than 0.02 are marked bold.

	Asymptotic test		M-SLRT test	
	Statistic	p-value	Statistic	p-value
Pumping time				
Cold open, decoupled, 0.3 min, He rich vs	0.191	0.662	0.229	0.632
Cold open, decoupled, 12 min, He rich Cold open, decoupled, 0.3 min, He rich vs	7.588	0.00587	8.61688	0.00333
Cold open, decoupled, 0.3 min, He rich	7.588	0.00587	8.01088	0.00333
Cold open, decoupled, 0.3 min, He rich vs	9.5024	0.00205	11.343	0.000756
Cold open, decoupled, 32 min, He rich	7.3024	0.00203	11.545	0.000730
Cold open, decoupled, 12 min, He rich vs	6.625	0.010054	6.236	0.0125
Cold open, decoupled, 22 min, He rich	0.025	0.010001	0.250	0.0120
Cold open, decoupled, 12 min, He rich vs	8.984	0.00272	8.793	0.00302
Cold open, decoupled, 32 min, He rich				
Gas composition during catalyst formation				
Cold open, decoupled, 0.3 min, He rich vs	0.3208	0.57108	0.298	0.585
Cold open, decoupled, 0.3 min, H2 rich				
Cold open, decoupled, 12 min, He rich vs	0.155	0.693	0.114	0.735
Cold open, decoupled, 12 min, H2 rich				
Cold open, decoupled, 32 min, He rich vs	1.5489	0.2132	1.463	0.2263
Cold open, decoupled, 32 min, H2 rich				
Reactor opening temperature				
Cold open, decoupled, 12 min, He rich vs	1.589	0.213	1.04	0.3077
Hot open, decoupled, 12 min, He rich				
Cold open, decoupled, 22 min, He rich vs	1.376	0.24	1.367	0.242
Hot open, decoupled, 22 min, He rich	1.010221	0.2140	0.042	0.2214
Cold open, decoupled, 32 min, He rich vs	1.010331	0.3148	0.943	0.3314
Hot open, decoupled, 32 min, He rich Cold open, coupled, 12 min, He rich vs	1.359	0.243	1.3904	0.2388
Hot open, coupled, 12 min, He rich	1.559	0.243	1.3904	0.2366
Decoupled catalyst formation				
Hot open, decoupled, 12 min, He rich vs	8.399	0.0038	7.161	0.0075
Hot open, coupled, 12 min, He rich	0.577	3.0000	,	3.007.0
Cold open, decoupled, 12 min, He rich vs	0.886	0.346	0.691	0.406
Cold open, coupled, 12 min, He rich				
Cold open, decoupled, 32 min, He rich vs	0.204	0.652	0.160	0.689
Cold open, coupled, 32 min, He rich				

Table 3. Main statistics from AFM analyses of substrates before second ramping with different pumping times and results of statistical tests (two-sample t-test and CV equality test). P-values less than 0.05 are marked bold.

		Mean particle	Mean RMS	Mean particle		
		height [nm]	roughness [nm]	number density [µm <sup>-1</sup> ]		
0.3 min	Sample 1	7.96	1.83	1684		
pumping	Sample 2	7.66	1.86	1713		
	Sample 3	8.07	1.91	1291		
	Average	7.90	1.87	1563		
32 min pumping	Sample 1	6.81	1.58	1732		
	Sample 2	5.76	1.30	1241		
	Sample 3	6.99	1.50	1356		
	Average	6.52	1.46	1443		
t-test						
t-statistic		3.42	4.77	0.5928		
p-value		0.027	0.009	0.5852		
CV equality test (asymptotic)						
statistic		2.77	3.28	0.0527		
p-value		0.096	0.070	0.8184		
CV equality test (M-SLRT)						
statistic		2.34	2.93	0.0170		
p-value		0.126	0.087	0.8962		

# **Table of Content Figure**



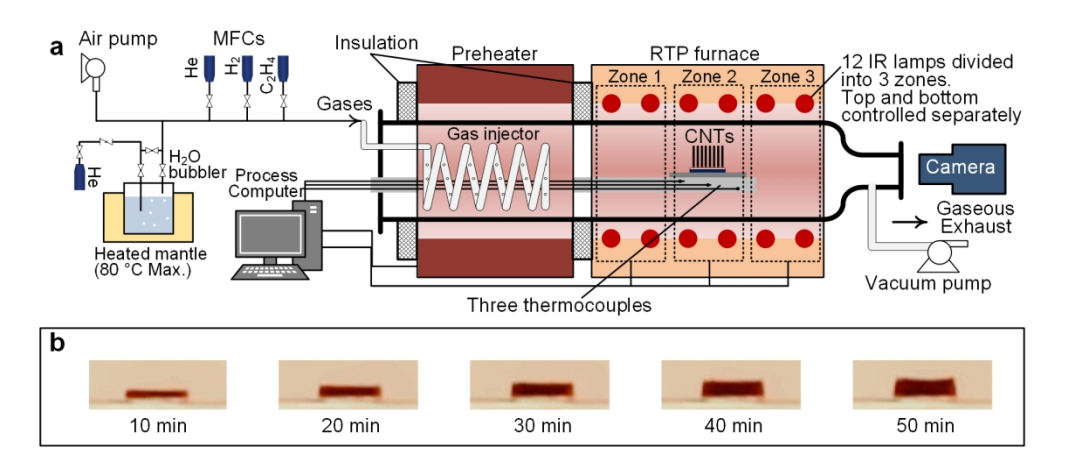


Fig. 1. (a) Schematic representation of the RTP CVD reactor used in this work. (b) Snapshots of a CNT forest growing in the reactor recorded by the video camera (sample size  $\approx 10 \times 10$  mm2).

161x68mm (300 x 300 DPI)

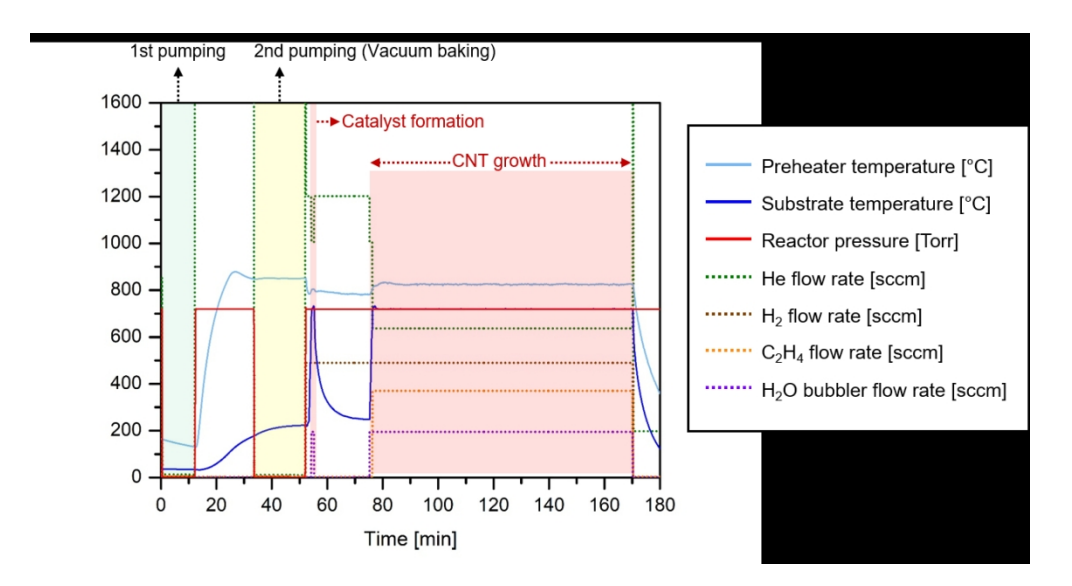


Fig. 2. A typical decoupled dynamic recipe used in this work. The recipe includes first pumping, second pumping at around 200 °C, a decoupled catalyst formation step, and CNT growth step.

218x116mm (150 x 150 DPI)

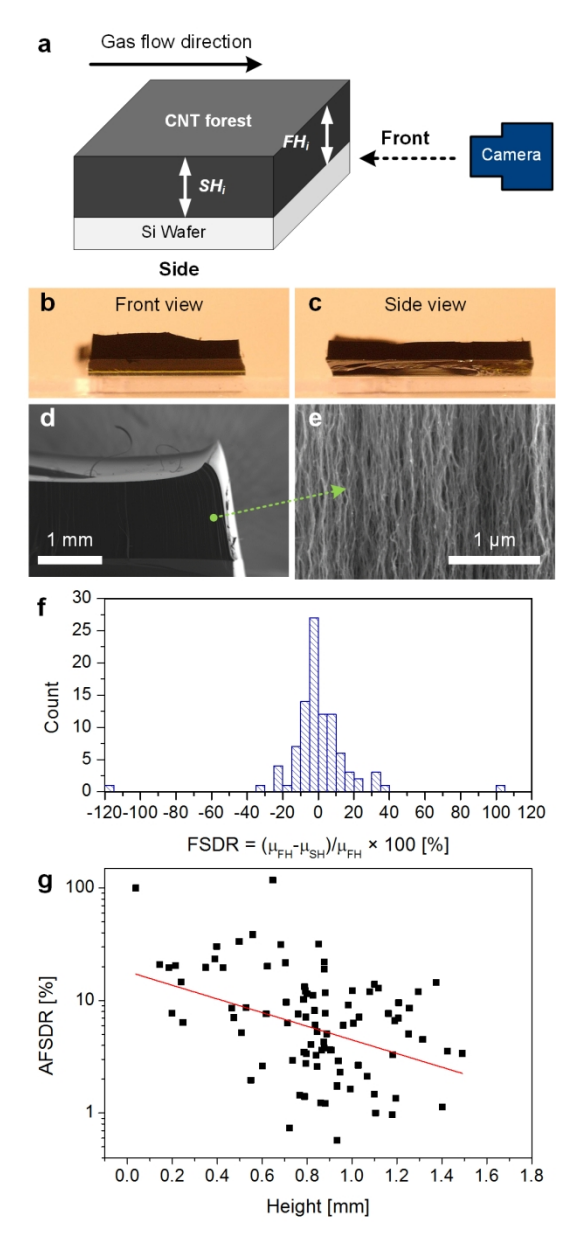


Fig. 3. (a) Schematic showing the forest height measurements from two different sides. (b) Front and (c) side view optical image of a typical CNT forest. (d, e) SEM images of a typical CNT forest. (f) Histogram of FSDR of CNT forests. (g) Plot of absolute values of FSDR as a function of forest height, showing the negative correlation. The red line is the linear regression line (R2 = 0.116).

88x198mm (300 x 300 DPI)

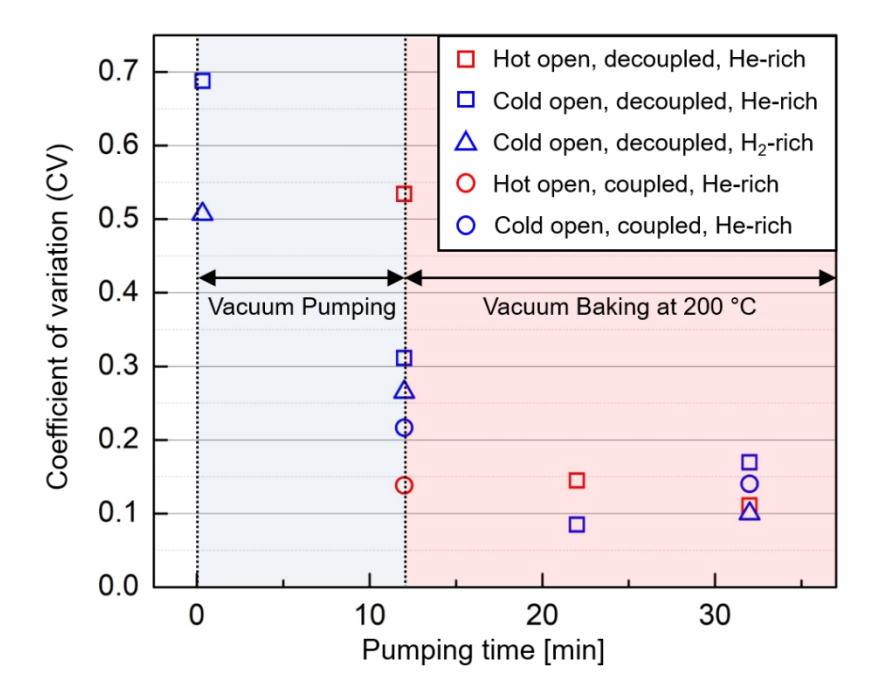


Fig. 4. CV of height of CNT forests synthesized from various growth recipes described in Table 1.  $204 \times 157 \, \text{mm} \, (150 \times 150 \, \text{DPI})$ 

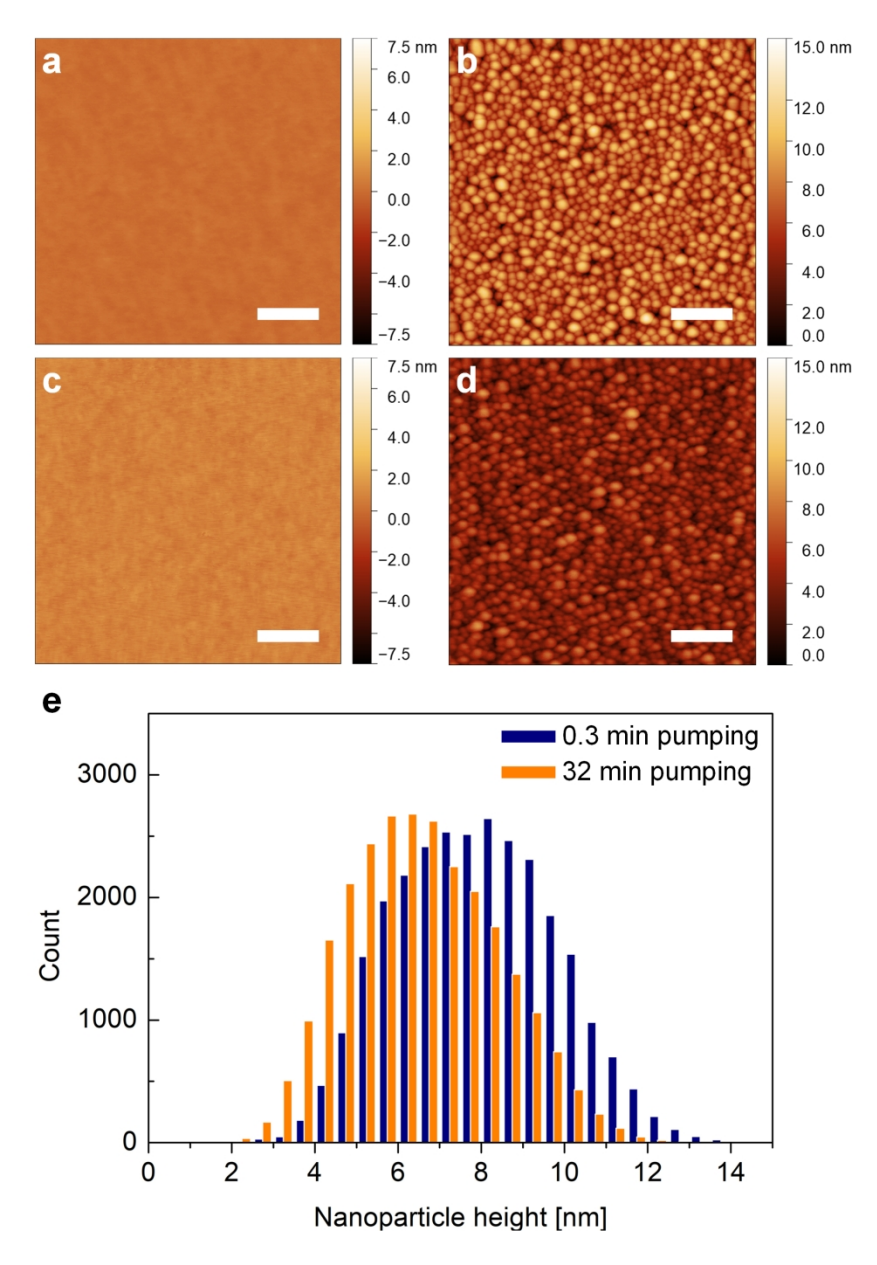


Fig. 5. (a, b) Representative AFM images of substrates after different treatments after pumping down for 0.3 minutes: (a) before catalyst preparation step and (b) after catalyst preparation step. (c, d) Representative AFM images of substrates after different treatments after pumping down for 32 minutes: (c) before catalyst preparation step and (d) after catalyst preparation step. Scale bars are 200 nm. (e) Histogram of nanoparticle heights after the catalyst preparation step for different pumping times (0.3 and 32 minutes).

179x253mm (300 x 300 DPI)

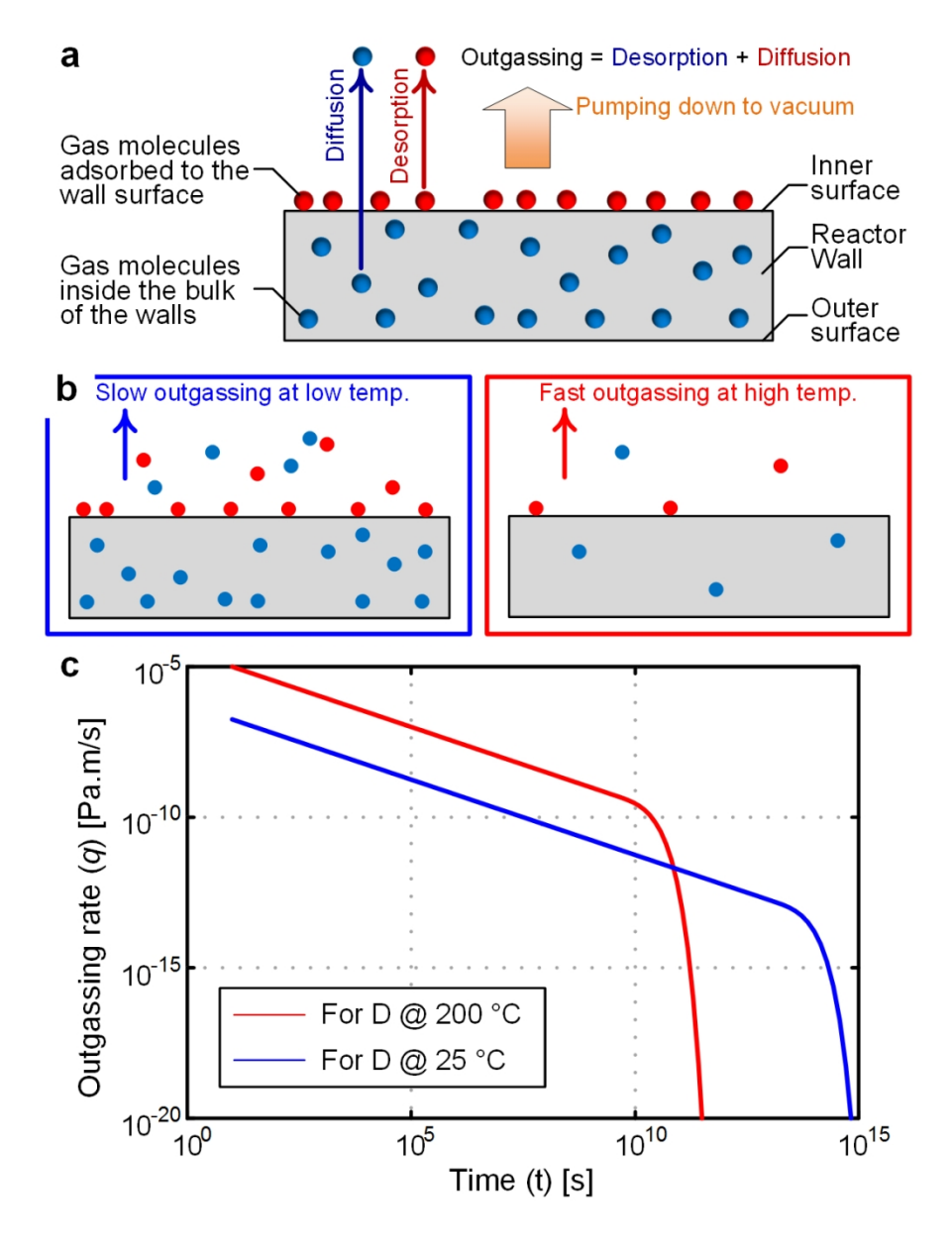


Fig. 6. (a)-(b) Schematic representations of outgassing: (a) Outgassing includes desorption from the wall surface and diffusion from inside the bulk of the wall; (b) Slow outgassing at low temperature and fast outgassing at high temperature. (c) Outgassing rate vs. time with two different diffusion coefficients: D = 10-18 m2 s-1 at 25 °C and D = 10-14.5 m2 s-1 at 200 °C. The diffusion coefficients are estimates for water diffusion through silica glass. For the calculation, we assumed C0 = 105 Pa and d = 10-4 m.

103x137mm (300 x 300 DPI)